Photocatalytic Degradation of Penicillin v Using Bi$_2$O$_3$/Ag/TiO$_2$ Thin Film in a Spinning Disc Photoreactor under Blue LED Illumination

Zamani, Sahar; Rahimi, Mahmood Reza*+

Process Intensification Laboratory, Department of Chemical Engineering, Yasouj University, Yasouj, I.R. IRAN

Ghaedi, Mehrorang

Department of Chemistry, Yasouj University, Yasouj, I.R. IRAN

ABSTRACT: *In this study, a novel Spinning Disc Photo Reactor (SDPR) was designed for the treatment of penicillin v (PV) as objective contaminants under blue Light-Emitting Diodes (LEDs) irradiation. To this end, a visible light-activated Bi$_2$O$_3$/Ag/TiO$_2$ catalyst thin film was deposited onto the surface of ceramic disc support through a facile sol-gel spin coating technique. The synthesized film is fully characterized by X-Ray Diffraction (XRD), Field Emission Scanning Electron Microscopy (FESEM), Energy-Dispersive Spectrometry (EDS), and Diffuse Reflectance Spectroscopy (DRS)techniques. A Central Composite Design (CCD) was exploited to optimize the operative variables including illumination time, rotational speed, initial PV concentration, and solution flow rate. The PV photodegradation efficiency of 97.67% was achieved at optimal operational conditions involving 80 minutes of illumination time, a rotational speed of 180 rpm, an initial PV concentration of 30 mg/L, and a solution flow rate of 0.8 L/min. Furthermore, the Langmuir-Hinshelwood (L–H) kinetic model fitted the empirical data well. Findings indicated that the developed SDPR can be a prominent alternative technology for the PV degradation process from wastewater.*

KEYWORDS: *Spinning disc reactor; Ceramic; Bi$_2$O$_3$/Ag/TiO$_2$ catalyst; Penicillin v; Blue LED illumination; Central composite design.*

INTRODUCTION

The presence of antibiotics in the aquatic environment has become an emerging environmental issue of concern that scientific researchers are trying to resolve [1]. Due to their biological activity in aquatic systems, this kind of pollutant poses a large threat to the life of humans, animals, and the aquatic environment in general [2-4].

Therefore, the disposal of drug pollutants in wastewater before its unregulated discharge into the environment has received massive devotion in environmental science. To this end, the Advanced Oxidation Process (AOP) is one of the treatment methods, which has been accepted as an effective approach to the degradation of antibiotics

pollutants owing to its saving energy, high efficiency, and low cost [5, 6]. Among various semiconductors, titanium dioxide (TiO_2) is the most widely used photocatalyst due to its unique properties such as high stability, low cost, relatively low toxicity, and excellent photocatalytic performance in comparison to other semiconducting materials [7]. However, TiO_2 as a photocatalyst, is compromised by some intrinsic limitations such as the recombination of electron-hole pairs, and poor light-harvesting ability that is restricted only to the ultraviolet (UV) region [8, 9]. There has been massive attention to improving the photocatalytic activity of TiO_2 by narrowing the band-gap energy for the utilization the visible light irradiation [10-12]. Thus, coupling TiO_2 with other semiconductors is a feasible method to overcome the photochemical corrosion of TiO_2 and could induce a high photocatalytic performance. Among various semiconductors, the significant attention to Bi−compounds among of different semiconductors is due to their high degradation rate of various pollutants [13, 14]. Among various metals, silver (Ag) has been widely used as a dopant to modify the electronic structures of TiO_2, due to its intrinsic narrow bandgap and visible light absorption capabilities [15, 16]. Designing a photocatalytic reactor is quite challenging in terms of the dependence of its photocatalytic performance on light harvesting. In the field of photocatalysis, the type of light source plays a vital role in catalyst activation and energy consumption. The UV spectrum has been the chief source of irradiation. However, it suffers from some downsides, including high cost, substantial heat generation, toxic by-products, poor mechanical resistance, and a short lifetime [17]. To resolve the mentioned defects numerous researchers have focused on the design of innovative photoreactors operating by visible light (e.g. Light-Emitting Diodes (LEDs)) recently, [18, 19] due to their high energy efficiency, low maintenance cost, long operating life, and low electricity consumption as compared to conventional light sources [20, 21]. The reported photocatalytic reactors are mostly in the slurry procedure from the literature, and few of the investigated immobilized photocatalytic reactors [22-26]. The slurry mode requires catalyst separation and recycling at the end of the photocatalytic reaction which may raise the operational costs and decline the mass transfer rate and reaction performance [27]. Furthermore, high concentrations of the catalyst may reduce the penetration

depth of light, produce secondary pollutants, and decline the accessibility of active sites for contaminants [28]. Thin films overcome these limitation issues and bear many advantages over powders such as the decrement of agglomeration and increasing of catalytic activity without using a high amount of material. Additionally, thin-film photocatalysts have been highly interesting because of their simple preparation, low−cost, applying different substrates, and eco–friendly. The immobilization of catalyst on such ceramic substrate could offer numerous advantages including large specific surface area, superior photocatalytic activity, proper adhesion to the photocatalysts, self-cleaning, resistance against high calcination temperatures, excellent mechanical features, chemical inertness toward both catalyst and contaminants, cost-effectiveness, and corrosion resistance [29, 30]. Therefore, in this research, ceramic support was selected for immobilizing the catalyst due to the reasons above. The deposition of a photocatalyst on the substrate can take place through several techniques such as sol-gel, dip-coating, photo-etching and spray pyrolysis, etc [31]. Compared to other chemical deposition techniques, the sol-gel approach has been one of the facile and promising approaches for thin film deposition due to its high efficiency, simple preparation, and cost-effectiveness [32]. The catalyst-immobilized reactors often suffer from mass transfer restrictions that can be resolved by using Spinning Disc Reactors (SDRs) with the catalyst immobilized on a rotating surface due to its highly sheared thin films with improved mass transfer performance, especially in solid-liquid systems [33-35]. Thus, in this study, a novel Spinning Disc Photocatalytic Reactor (SDPR) was designed and fabricated to optimize the depth of light penetration and external mass transfer improvement. The developed apparatus was equipped with blue LED lamps at a certain distance from the center of the spinning ceramic disc to compensate for the non-uniform light distribution by an effective light penetration depth to minimize the amount of light exposure for the catalyst activation. The photocatalytic performance of the proposed SDPR was evaluated for degradation of PV in an aqueous solution under a set of optimized conditions obtained by the Central Composite Design (CCD) under visible blue light irradiation. FESEM, EDX, XRD, and UV Visible spectroscopy systematically characterized the synthesized thin film. Understanding the effects of various

parameters on photocatalytic degradation efficiency is crucial and design and operational perspectives are important in selecting a sustainable and efficient treatment method for effluent treatment. The influences of illumination time, rotational speed, initial concentration of PV, and solution flow rate on the photocatalytic degradation efficiency of PV were discussed. The reusability and stability experiments of the novel synthesized photocatalyst in PV degradation were fulfilled in several cycles.

EXPERIMENTAL SECTION
Materials and reagents

Tetra butyl ortho-titanate (TBOT, $C_{16}H_{36}O_4Ti$), isopropanol (C_3H_8O), bismuth nitrate pentahydrate ($Bi(NO_3)_3.5H_2O$), ethanol (C_2H_5OH), hydrochloric acid (HCL), sodium hydroxide (NaOH), silver nitrate ($AgNO_3$) and chemical oxygen demand (COD) vial were supplied from Merck Company (Germany). Polyvinylpyrrolidone (PVP) powder was provided by Sigma-Aldrich (USA). Penicillin V (PV, $C_{16}H_{18}N_2O_5S$) was purchased from Farabi Pharmaceutical Company (Iran). Deionized water was provided from the Milli-Q system (Millipore, Bedford, MA, USA) and used as the solvent. The mentioned reagents were applied with no further purification.

Preparation of photocatalyst film

The $Bi_2O_3/Ag/TiO_2$ thin film was deposited onto the ceramic disc via a facile sol-gel spin coating route. To prepare the precursor solution, initially, 0.2 g PVP was added to 10 ml isopropanol and mixed at ambient temperature for 20 min. Afterward, 2.50 ml TBOT was added to the above solution under 30 minutes of stirring at room temperature to reach a transparent and homogeneous TiO_2 solution. In the next stage, 1.36 g bismuth nitrate pentahydrate and 0.35 g silver nitrate were dissolved in double-distilled water and added to the reaction mixture (using a dropper) under vigorous stirring for 2 h until a stable solution was achieved. Prior to deposition, the ceramic disc substrate was cleaned, followed by preheating. The second step involved the coating of the ceramic disc through a spin-coater operating at 700 rpm for 60 seconds followed by drying at room temperature under a fume hood. Then, the coated films were rinsed with distilled water to eliminate any unattached particles, followed by drying at ambient temperature for 10 h. Finally, the as-prepared films were annealed at 600 °C for 5 h to enhance

their adhesion to the ceramic substrate and eliminate the residual organic components. The heating rate was set at 2 ◦C/min to avoid cracking. The spin coating step was repeated several times to attain multi-layer films with higher amounts of catalysts.

Characterization techniques

The prepared catalyst films were characterized to educate their physicochemical properties. The crystal structure of the catalysts was conducted by X-Ray Diffractometer (XRD, Philips PW 1800, Cu kα, voltage of 40 kV, and 40 Ma) in the 2θ range of 20°-80°. The optical absorption of the dye solution was evaluated using UV-Vis spectroscopy (V-530, Jasco, Japan). The surface morphological properties of the specimens were assessed by Field Emission Scanning Electron Microscopy (FESEM: Sigma, Zeiss) equipped with an Energy Dispersive X-ray (EDS) Spectrophotometer to examine the chemical composition of the samples. Diffuse Reflectance Spectroscopy (DRS, Avant Avaspec-2048-TEC) was also applied. The pH of the solutions was measured by a pH meter (AL 20).

Fabrication of Spinning Disc Photocatalytic Reactor (SDPR)

A Spinning Disc Photocatalytic Reactor (SDPR) was successfully designed and fabricated based on semi-continuous mode and used for the PV photodegradation in wastewater samples as shown in Fig. 1. The designed experimental setup included four prominent components: cylindrical glass vessel (height=50 cm, diameter = 22.5 cm, and thickness=10 mm), a spinning ceramic disc (thickness=2 mm and diameter= 20 cm), a solution distributor (8 holes with a diameter of 2 mm), and blue LED lamps (7 W, 465 nm). Furthermore, the reactor system also encompassed several components such as a motor, aeration pump, flow meter, reservoir tank, stirrer, liquid pump, control valves, sampler valve, and control panel. The disc was coupled to a shaft to be driven by an electric engine. A frequency converter could tune the spinning rate of the ceramic disc. The liquid feed was distributed onto the ceramic disc through a liquid distributor. Six blue LED lamps were embedded into the glass disc to serve as the light illumination source for the photocatalytic process. The uniform light distribution and an efficient permeation depth were ensured by locating
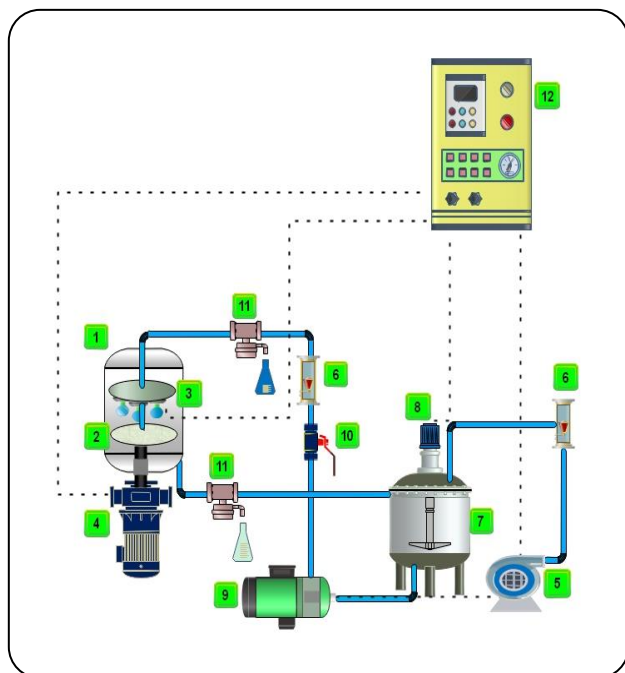
Fig. 1: Spinning disc photocatalytic reactor set-up, 1: Reactor vessel, 2: Spinning ceramic disc, 3: LED light source, 4: Motor, 5: Aeration pump, 6: Flowmeter, 7: Reservoir, 8: Stirrer, 9: Liquid pump, 10: Control valve, 11: Sampler valve, 12: Control box.
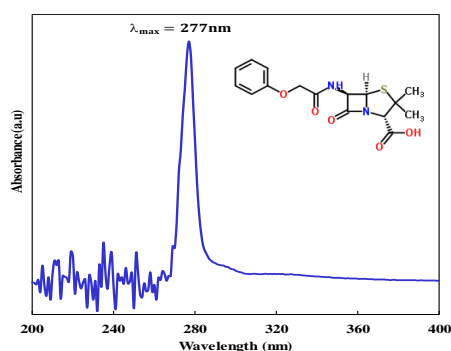
Fig. 2: UV-Vis absorption spectrum of PV in distilled water.

the LED lamps at a short distance above the spinning ceramic disc. The photocatalytic performance of the proposed SDPR system was monitored by the degradation of PV as a target contaminant with $Bi_2O_3/Ag/TiO_2$ thin film immobilized onto ceramic disc substrate under visible light illumination. In a typical experiment, a certain amount of PV powder was added to deionized water under vigorous stirring. The pH was then set by 0.1 M HCl and 0.1 M NaOH solutions. The reactor was entirely cleaned

with distilled water before the experiments. Then, the stirred tank reservoir was charged with PV solution at varying concentrations. The aeration pump was responsible for supplying the oxygen for the photocatalytic reaction. The PV solution from the stirred tank reservoir was then transferred to the center of the spinning ceramic disc by a liquid distributor. The photocatalytic experiments were run by complete reuse of the reservoir tank through gravity.

Moreover, the photolysis of PV solution and the light dispersion were avoided by covering the tank reservoir and the cylindrical glass vessel with an aluminum foil. The employed reactant volume was 2500 mL of aqueous PV solution. Before irradiation, the adsorption-desorption balance was attained by 30 min rotation of the $Bi_2O_3/Ag/TiO_2$ coated ceramic disc at the speed of 100 rpm at the darkness. Then, the LED illumination was turned on, and the photocatalytic reaction was initiated. During the photocatalytic reaction, 3 ml of solution was withdrawn from the sampler valve at the given intervals. The PV concentration was measured by the UV-Vis absorption curve at 200-600 nm. The photodegradation percentage can be estimated by:

$$P\% = \frac{C_0 - C_t}{C_0} \times 100 \qquad (1)$$

in which, *P* shows the photodegradation percentage of PV (%), and C_0 and C_t denote the PV concentration at the beginning of the procedure and the certain time (*t*), respectively. The characteristic UV-Vis absorption peak of PV in water is depicted in Fig. 2.

Design of experiments

Experimental design for the photocatalytic degradation of PV was carried out using the Central Composite Design (CCD) based on the Response Surface Method (RSM), a collection of statistical and mathematical techniques useful for optimizing the processes. RSM can investigate the effect of individual and combination interactions of operational parameters on the photocatalytic degradation efficiency [36]. Therefore, the influence of four prominent variables consists of illumination time (X1), rotational speed (X2), PV concentration (X3), and solution flow rate (X4), were investigated using CCD, and a totally 21 experimental runs were provided. The levels of the studied factors (high, low, center, and star points) are listed in Table 1.

Table 1: Levels of factors in CCD.

Factors	Levels				
	Low (-1)	Central (0)	High (+1)	-α	+α
X_1: Illumination Time (min)	40	60	80	20	100
X_2: Rotational Speed (rpm)	80	130	180	30	230
X_3: PV Concentration (mg/L)	20	30	40	10	50
X_4: Solution Flow rate (L/min)	0.6	0.8	1.0	0.4	1.2

Table 2: CCD matrix and response.

Run	X_1	X_2	X_3	X_4	P% $_{PV}$
1	60	130	10	0.8	86.23
2	40	80	20	0.6	62.31
3	60	130	30	0.4	90.05
4	60	130	50	0.8	79.12
5	100	130	30	0.8	97.13
6	80	180	20	1.0	84.86
7	40	80	20	1.0	93.01
8	80	80	40	1.0	68.22
9	60	130	30	0.8	92.99
10	60	30	30	0.8	61.44
11	60	130	30	0.8	92.84
12	40	180	40	0.6	82.39
13	60	130	30	0.8	92.03
14	80	180	20	0.6	95.85
15	60	130	30	0.8	92.74
16	40	180	40	1.0	67.85
17	60	230	30	0.8	91.84
18	60	130	30	0.8	92.35
19	60	130	30	1.2	76.82
20	20	130	30	0.8	65.76
21	80	150	40	0.6	90.15

Design-Expert 10.0 software was employed to analyze the experimental results. The design matrix included 21 experimental runs for four variables at five levels (−α, −1, 0, +1, and +α) and was analyzed by ANOVA as presented in Table 2. A quadratic polynomial model equation was implemented to explore the interactive impacts between the independent variables and their corresponding responses. The model equation can be expressed as:

$$Y = \beta_0 + \sum_{i=1}^{4} \beta_i X_i + \sum_{i=1}^{4} \sum_{j=1}^{4} \beta_{ij} X_i X_j + \sum_{i=1}^{4} \beta_{ii} X_i^2 + \varepsilon \quad (2)$$

in which Y shows the predicted response; while X_i and X_j denote the independent variables. β_0, β_i, β_{ii}, β_{ij}, and ε also stand for the constant, linear, quadratic, and interaction coefficients and the residual term, respectively. The significance of the quadratic model was examined
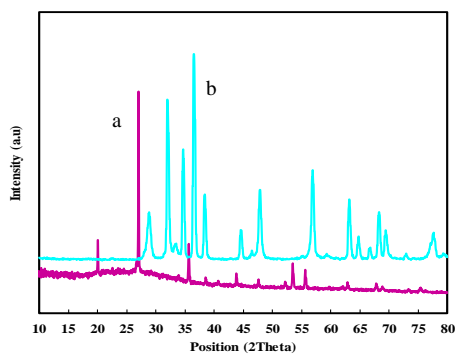
Fig. 3: XRD pattern of (a) ceramic disc before doping, (b) Bi₂O₃/Ag/TiO₂ catalyst film.

by an ANOVA analysis in terms of the F-value, P-value, lack of fit criteria regression correlation squared (R^2), adjusted R-squared (R^2 adj.), predicted R-squared (R^2 pred.), and the Predicted Residual Error Sum Of Squares (PRESS).

RESULTS AND DISCUSSION

Characteristics of the ceramic substrate and the thin films

The XRD patterns of the ceramic substrate and the thin film sample are shown in Fig. 3. The XRD pattern in Fig. 3a shows the important phases of ceramic: Zircon, Sillimanite (JCPDS card No. 01-088-0893), and anatase TiO_2 (JCPDS card No. 21-1272). As seen, the main diffraction peaks were located at 2θ=20.0°, 26.96°, 33.81°, 35.61°, and 55.60° well corresponding to the (1 0 1), (2 0 0), (2 1 1), (1 1 2) and (2 1 3) crystal planes of Zircon, respectively (JCPDS card No. 72-0402). The peaks located at 52.30°, 53.45°, and 75.36° are the characteristic diffraction peaks of (1 4 1), (0 2 3), and (4 2 3) planes which can be well indexed as the Sillimamite phase, respectively (JCPDS card No. 01-088-0893). Some minor diffraction peaks at 38.51° also corresponded to (1 1 2) plane in the anatase TiO_2(JCPDS card No. 21-1272). Fig. 3. b represents the XRD patterns of Bi_2O_3/Ag/TiO_2 film. In the case of the TiO_2 film, the diffraction peaks are ascribed to (1 0 1), (0 0 4), (2 0 0), (1 0 5), (2 1 1), (2 0 4), (1 1 6), (2 2 0), (1 0 7), (2 1 5) planes, which related to tetragonal phase of TiO_2 film (JCPDS PDF No 21-1272). From the XRD patterns, the peaks could be indexed to the (1 2 1), (0 2 2), (0 2 2), (311), and (1 0 4) crystal planes which related to Bi_2O_3 (Ref code 76-1730). In the case of the Ag nanoparticles, the peaks at 38.11∘, 44.30∘, 64.44∘, and 47.40∘ could be indexed to the (111), (0 0 2), (0 2 2), and (13) crystal planes which related to Cubic phase of Ag

nanoparticles (Ref code 96-500-0219).

The morphologies of the substrate and the Bi_2O_3/Ag/TiO_2 thin film were examined using FESEM as depicted in Fig. 4. The ceramic substrate possessed a porous surface morphology with lots of valleys and screws offering a substantial surface area for immobilizing the catalyst film (Fig. 4a). The substrate coated with Bi_2O_3/Ag/TiO_2 presented a film layer with an irregular texture with finer particle size (Fig. 4b). This result demonstrates that the Bi_2O_3/Ag/TiO_2 film with a small size promoted the light absorption capability and enhanced the catalyst-pollutant interface, hence, improving the photocatalytic activity during the degradation process. Therefore, high active sites were formed on Bi_2O_3/Ag/TiO_2 surface for the PV degradation under visible light.

The chemical composition of the ceramic substrate and catalyst films was examined by EDS. The EDS results indicated the presence of Si, O, Ti, Zr, Al, K, Na, and Ca elements in the ceramic substrate structure (Fig. 4c), while the EDS analysis of Bi_2O_3/Ag/TiO_2 films proved the effective doping due to the presence of Ti, O, Bi and Ag (Fig.4d). Moreover, the light absorption of samples was recorded by UV-vis diffuse reflectance spectra. Fig.5 suggests that both TiO_2 and Bi_2O_3/Ag/TiO_2 exhibited light absorption from UV to the visible light region (200-900 nm). The below equation can calculate the band-gap of the samples:

$$(\alpha h\upsilon)^2 = B(h\upsilon - E_g) \tag{3}$$

in which α, h, υ, B and E_g denote the absorption coefficient, plank constant, photon frequency, a proportionality constant, and the energy band-gap, respectively. The direct band-gap of the photocatalysts can be determined from the intercepts of the straight lines at α = 0. The bandgaps of TiO_2 and Bi_2O_3/Ag/TiO_2 were determined as ∼3.2 eV and 1.91 eV, respectively (Fig. 5).

With the deposition of Ag nano particles (NPs) heterojunctions further show more intense absorption in visible light region, which can be attributed to the surface plasmon resonance (SPR) of Ag metal NPs. The results revealed that the Bi_2O_3/Ag/TiO_2 could be used as a promising catalyst for visible light photocatalysis due to its high generation of photo-generated electrons and holes.

Statistical analysis and model fitting

The significance of the model parameters including individual or their interaction, could be confirmed based
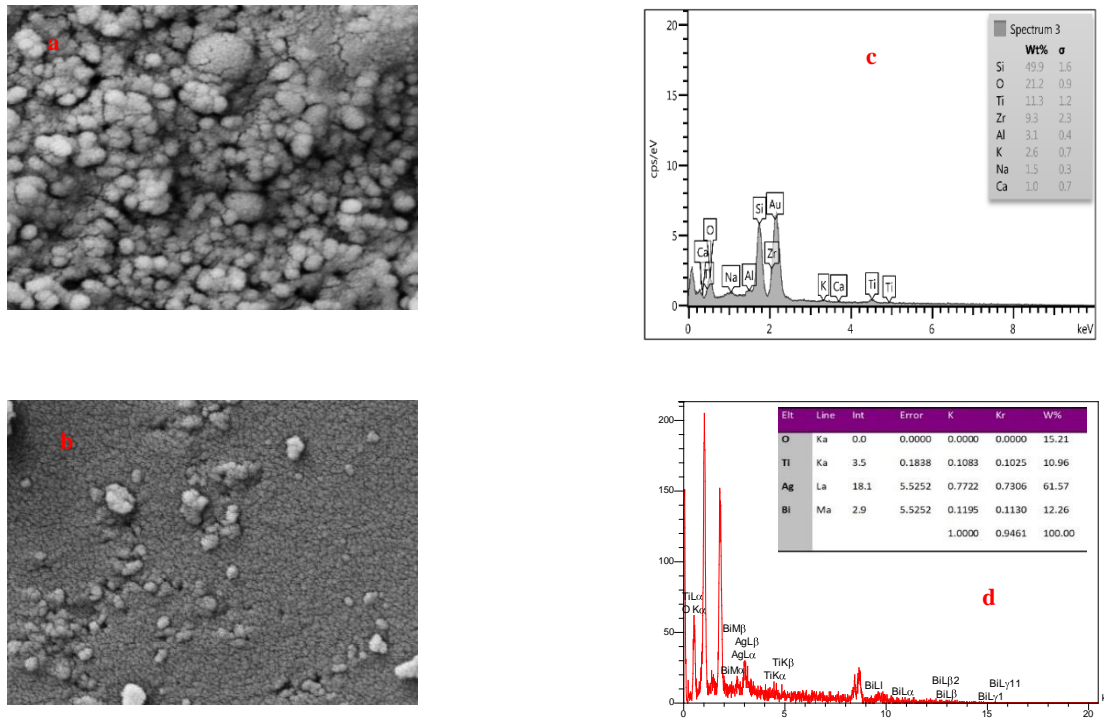
Fig. 4: FE-SEM images: (a) raw ceramic disc substrate, (b) the Bi₂O₃/Ag/TiO₂ thin film, EDS spectrum of: raw ceramic disc substrate (c), the Bi₂O₃/Ag/TiO₂ thin film (d).
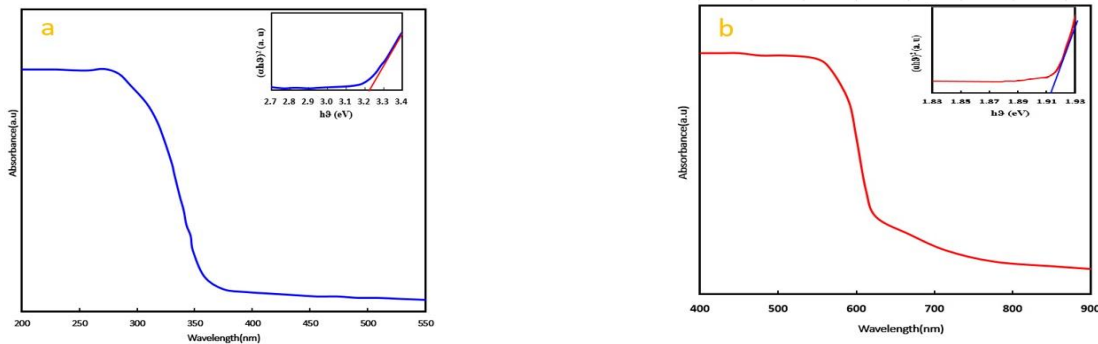
Fig. 5: DRS spectra (a) TiO₂ film and (b) Bi₂O₃/Ag/TiO₂ film.

on the following criteria: p-value<0.05 and lack of fit>0.05 for each factor in the model. Based on the ANOVA analysis, the quadratic model was accepted as the best-fitted model to the obtained experimental data of PV photodegradation percentage with appropriate quality and reliable aforementioned statistical criteria (Table. 3). The corresponding F-value and lack-of-fit P-values of the PV degradation model were found to be 3204.77 and 0.091, respectively, which were proved the significance

of the applied model. The developed quadratic model with significant parameters for the prediction of photocatalytic degradation percentage was obtained as follow:

$$P\%_{PV} = 92.04 + 10.51X_1 + 3.83X_2 + 5.77X_3 + 2.40X_4 + 2.47X_1X_2 + 1.48X_1X_3 + 2.64X_1X_4 - 1.25X_2X_3 - 0.51X_2X_4 - 3.60X_1^2 - 3.51X_2^2 - 3.53X_3^2 - 1.38X_4^2 \qquad (4)$$

Table 3: ANOVA for quadratic model.

	DF[a]	SS[b]	MS[c]	F- Value	P-value
Model	14	2451.49	175.08	12.07	< 0.0001
X_1	1	641.18	641.18	44.20	< 0.0001
X_2	1	288.05	288.05	19.85	< 0.0001
X_3	1	32.49	32.49	2.24	< 0.0001
X_4	1	40.50	40.50	2.79	< 0.0001
X_1X_2	1	34.93	34.93	2.46	< 0.0001
X_1X_3	1	3.15	3.15	0.22	0.0001
X_1X_4	1	206.50	206.50	14.24	0.0001
X_2X_3	1	14.31	14.31	0.99	0.031
X_2X_4	1	134.68	134.68	9.28	0.038
X_3X_4	1	1.46	1.46	0.10	0.0019
X_1^2	1	195.69	195.69	13.49	< 0.0001
X_2^2	1	1057.48	1057.48	72.90	< 0.0001
X_3^2	1	75.45	75.45	5.19	< 0.0001
X_4^2	1	140.51	140.51	9.69	< 0.0001
Residual	6	87.03	14.53		
Lack of Fit	2	86.98	0.49	3204.77	0.091
Pure Error	4	0.054	0.014		
Cor Total	20	2538.04			

3D-surface plots

The relationship between the operational parameters and the response was depicted by the three-dimensional response surface plots, which can describe the individual and combinational interaction of effective operational parameters on the photocatalytic degradation process of PV as the response (Fig. 6). In all experiments, a constant aeration rate was fed to the solution tank to provide the required oxygen to increase the photocatalytic degradation efficiency. Fig. 6a shows the interactive effect of the illumination time and solution flow rate on the PV photodegradation. The solution flow rate is an effective factor that could affect the photodegradation process either positively or negatively. As can be seen from Fig. 6a, the degradation efficiency showed an enhancement by increasing the flow rate from 0.4 to 0.8 L/min. This may be assigned to higher passes of a reactants molecule to the spinning disc at a higher flow rate, influencing the reaction rate. However, a further increase in the flow rate lowered the degradation efficiency due to the reduction in the resistance time of reactants, high liquid film thickness, and

decrease of the light penetration [37]. Moreover, enhanced flow rates are correlated with a strong decrement in the contaminant-photocatalyst interfacial area and a significant reduction in the mass transfer rate [33]. The effect of LED illumination time on the PV degradation revealed that longer illumination durations increased the photocatalytic degradation as the pollutants will be more exposed to the illumination and produce more free radicals.

The rotational speed is one of the most impressive operation parameters affecting the photocatalytic reaction (See Fig. 6b). This factor is related to the thickness of the liquid film and the mass transfer coefficients of contaminates [37]. A remarkable increase was detected in the PV photodegradation efficiency with increasing the rotational speeds from 30 to 180 rpm. This phenomenon can be explained as follows: An increase in the disc rotation speed will boost the micromixing while reducing the mass transfer resistance and the formation of thin sheared liquid film and droplets on the disc surface, leading to a high interfacial area between the catalyst film/disc and contaminant [37, 38]. However, the PV
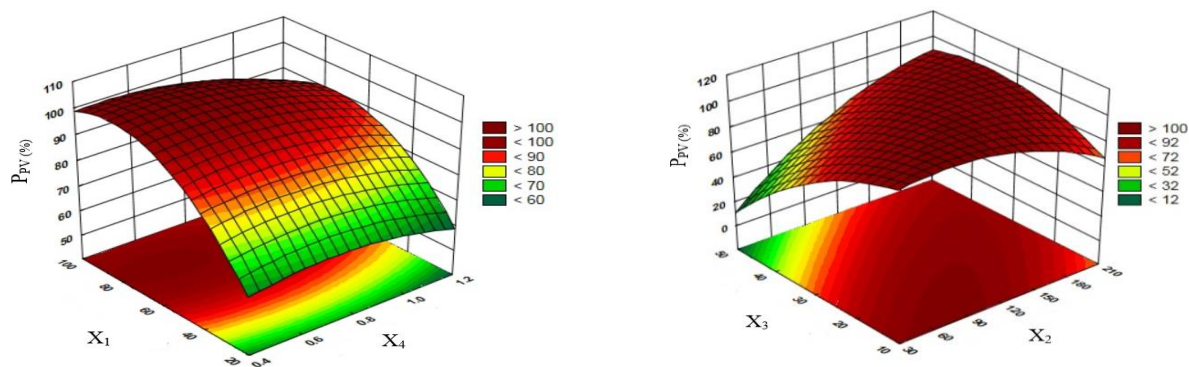
Fig. 6: Response surface (3D) plots for photocatalytic degradation of PV versus independent variables:
(a): Rotational speed with PV concentration, (b): Illumination time with solution flow rate.

degradation efficiency decreased with further increment of the rotational disc speed, which could be assigned to the decline of the liquid hold-up and residence time. The influence of pollutant concentrations on the photodegradation of PV was also addressed. Apparently, higher photodegradation efficiency was obtained at lower concentrations. Moreover, the PV removal rate showed a decline by enhancing PV concentration. This phenomenon could be assigned to the decrement of the number of accessible active sites per one PV molecule due to the adsorption site saturation and inadequate light exposure, reducing the photodegradation efficiency [39, 40].

Optimization of the photocatalytic process

Statistica software (version. 10) was applied to optimize of efficient independent variables in the PV photodegradation process using the desirability function. The range of DF variation was between 0–1 for undesirable and very desirable cases, respectively. The desirability value corresponds to the maximum photocatalytic degradation percentage was indicated that maximum degradation efficiency was 97.67%, at optimum values of 80 minutes of illumination time, a rotational speed of 180 rpm, initial PV concentration of 30 mg/L, and solution flow rate of 0.8 L/min. For checking the validity of the predicted values, the degradation experiment at optimum conditions was fulfilled three times where the average degradation percentage for three replicates was around 97.04 %, which showed the high accuracy prediction of the desirability function.

Kinetics of degradation

The Langmuir–Hinshelwood (L–H) as an accepted kinetic model for degradation of different types of organic compounds was used to explain the kinetics of photocatalytic degradation of PV as follow:

$$\ln\left(\frac{C_0}{C_t}\right) = k_c \tag{5}$$

where C_0 is the initial PV concentration, C_t shows the reactive concentration at the time of t, and k_c (min^{-1}) denotes the apparent rate constant. The experimental data were verified by plotting $\ln(C_0/C_t)$ versus t, whose slope indicates the apparent rate constant of the photocatalytic degradation (Fig. 7 a). The explanation of apparent photocatalytic degradation (R) at the solid-liquid interfaces can be fitted by L-H kinetic rate expression [40]:

$$R = -\frac{dC}{dt} = k_r\theta = k_r\frac{KC_0}{1 + KC_0 + K_sC_s} \tag{6}$$

where k_r, K, K_s, C_0, and C_s are the apparent photodegradation rate constant, the adsorption coefficient of the PV, adsorption coefficient of the solvent, and initial concentrations of the substrate and the solvent, respectively. K_A (L/ mg) is defined by:

$$K_A = \frac{K}{1 + K_sC_s} \tag{7}$$

After combining the equations, the photodegradation rate equation can be written as:

$$R = k_r\frac{K_AC_0}{1 + K_AC_0} \tag{8}$$

The L-H model can be investigated according to the plot of $1/R$ as a function $1/C_0$ (R and C_0 are the initial rate and initial PV concentrations, respectively) (Fig. 7b). The intercept and slope of this linear plot correspond to $1/k_r$ and $1/k_rK_A$, respectively. Based on Fig.7b, L-H
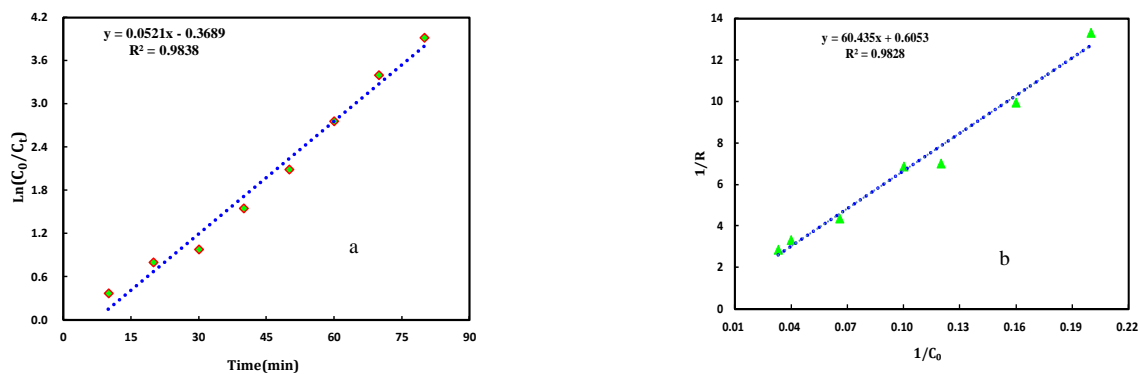
Fig. 7: Plot of the Langmuir-Hinshelwood (L-H) kinetics model for obtain apparent rate constant of processes at optimal conditions.
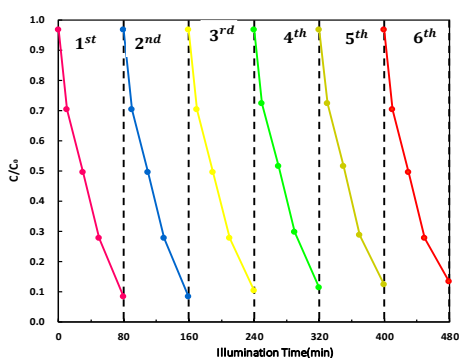

Fig. 8. Stability of the Bi₂O₃/Ag/TiO₂ catalyst film in the degradation of PV removal at optimal conditions.

kinetics model showed a proper fitting with experimental data of PV photocatalytic degradation. The photocatalytic reaction rate, L–H rate, and L–H adsorption constants were 0.0521 1/min, 1.625 mg L/min, and 0.0101 L/mg, respectively.

Stability and reusability of catalyst film experiments

The stability and reusability of the catalyst film are two major parameters in the practical implementation and economic cost of a photocatalytic reactor. To examine the stability of the prepared $Bi_2O_3/Ag/TiO_2$ thin film, several successive cycles were carried out for the degradation of PV under optimal conditions involving illumination time of 80 min, the rotational speed of 180 rpm, initial PV concentration of 30 mg/L, and solution flow rate of 0.8 L/min. In each experimental procedure, after the photocatalytic reactions, the catalyst film was washed with distilled water followed by 5 hours of oven-drying at 85 ℃. As obviously shown in Fig.8, no significant decline was observed in the photocatalytic activity of the

samples after six runs as they exhibited robust photocatalytic activity, implying the excellent reusability of this system. Consequently, the proposed SDPR could be regarded as a promising technology for contaminant degradation due to its proper photocatalytic behavior and high reliability.

CONCLUSIONS

In this study, an innovative SDPR was fabricated for the photocatalytic degradation of PV under blue light LED irradiation. The proposed reactor encompassed a spinning ceramic disc with immobilized $Bi_2O_3/Ag/TiO_2$ catalyst thin film. CCD was employed to design the experiments at an appropriate level of operation to save time and costs. The optimal conditions involved illumination time of 80 min, the rotational speed of 180 rpm, the solution flow rate of 0.8 L/min, and PV concentration of 30 mg/L. Under optimum conditions, the maximum PV photodegradation percentage (97.67 %) was obtained with the desirability of 0.923. Furthermore, kinetics studies revealed that a pseudo-first-order model based on Langmuir-Hinshelwood (L–H) could successfully fit the experimental data. Finally, the high stability and appropriate reusability of the synthesized heterojunction photocatalyst thin film were evidenced by repeating the photodegradation process for six cycles at optimum conditions. In general, the results revealed that the innovative SDPR system developed in the current research is a superior and robust technology for the photocatalytic degradation of PV.

REFERENCES

[1] Liu J.L., Wong M.H., Pharmaceuticals and Personal Care Products (PPCPs): A Review on Environmental Contamination in China, *Environ. Int.,* **59**: 208-224 (2013).

[2] Zhao C., Pelaez M., Duan X.D., Deng H.P., O'Shea K., Fatta-Kassinos D., Dionysiou D.D., Role of pH on Photolytic and Photocatalytic Degradation of Antibiotic Oxytetracycline in Aqueous Solution Under Visible/Solar Light: Kinetics and Mechanism Studies, *Appl. Catal. B*, **134-135**: 83-92 (2013).

[3] Lai, C. Zhang M., Li B., Huang D., Zeng G., Qin L., Liu X., Yi H., Cheng M., Li L., Chen Z., Chen L., Fabrication of CuS/BiVO$_4$ (0 4 0) Binary Heterojunction Photocatalysts with Enhanced Photocatalytic Activity for Ciprofloxacin Degradation and Mechanism Insight, *Chem. Eng. J.,* **358**: 1-18 (2019).

[4] Dimitrakopoulou D., Rethemiotaki I., Frontistis Z., Nikolaos P., Venieri D., Mantzavinos D., Degradation, Mineralization and Antibiotic Inactivation of Amoxicillin by UV-A/TiO$_2$ Photocatalysis, *J. Environ. Manage*, **98**: 168-174 (2012).

[5] Homem V., Santos L., Degradation and Removal Methods of Antibiotics from Aqueous Matrices e a Review, *J. Environ. Manage*, **92**: 2304-2347 (2011).

[6] Klavarioti M., Mantzavinos D., Kassinos D., Removal of Residual Pharmaceuticals from Aqueous Systems by Advanced Oxidation Processes, *Environ. Int.*, **35**: 402-417 (2009).

[7] Jiang L., Yuan X., Zeng G., Wu Z., Liang J., Chen X., Leng L., Wang H., Metal-Free Efficient Photocatalyst for Stable Visible-Light Photocatalytic Degradation of Refractory Pollutant, *Appl. Catal. B*, **221**: 715–725 (2018).

[8] Shayegan Z., Lee C.S., Haghighat F., TiO$_2$ Photocatalyst for Removal of Volatile Organic Compounds in Gas Phase – A Review, *Chem. Eng. J.,* **334**: 2408-2439 (2018).

[9] Song J., Wang X., Ma J., Wang X., Wang J., Xia S., Zhao J., Removal of Microcystis Aeruginosa and Microcystin-LR Using a Graphitic-C$_3$N$_4$/TiO$_2$ Floating Photocatalyst under Visible Light Irradiation, *Chem. Eng. J.,* **348**: 380-388 (2018).

[10] Dosado A.G., Chen W.T., Chan A., Sun-Waterhouse D., Waterhouse G.I.N., Novel Au/TiO$_2$ Photocatalysts for Hydrogen Production in Alcohol–Water Mixtures Based on Hydrogen Titanate Nanotube Precursors, *J. Catal.*, **330**: 238-254 (2015).

[11] Gong Y., Wu Y., Xu Y., Li L., Li C., Liu X., Niu L., All-solid-state Z-scheme CdTe/TiO$_2$ Heterostructure Photocatalysts with Enhanced Visible-Light Photocatalytic Degradation of Antibiotic Waste Water, *Chem. Eng. J.,* **350**: 257-267 (2018).

[12] Sayed M., Arooj A., Shah N.S., Khan J.A., Shah L.A., Rehman F., Arandiyan H., Khan A.M., Khan A.R., Narrowing the Band Gap of TiO$_2$ by Co-Doping with Mn^2+ and Co^2+ for Efficient Photocatalytic Degradation of Enoxacin and Its Additional Peroxidase Like Activity: A Mechanistic Approach, *J. Mol. Liq*, **272**: 403–412 (2018).

[13] Chen Z.P., Mou K.W., Wang W.H., Liu L.C., Nitrogen-Doped Graphene Quantum Dots Enhance the Activity of Bi$_2$O$_3$ Nanosheets for Electrochemical Reduction of CO$_2$ in a Wide Negative Potential Region, *Angew. Chem. Int. Ed.,* **57**: 12790-12794 (2018).

[14] He W.J., Sun Y.J., Jiang G.M., Huang H.W., Zhang X.M., Dong F., Activation of Amorphous Bi$_2$WO$_6$ with Synchronous Bi Metal and Bi$_2$O$_3$ Coupling: Photocatalysis Mechanism and Reaction Pathway, *Appl. Catal. B: Environ.*, **232**: 340–347 (2018).

[15] Xu H., Xie J., Jia W., Yu G., Cao Y., The Formation of Visible Light-Driven Ag$_2$O/Ag Photocatalyst with Excellent Property of Photocatalytic Activity and Photocorrosion Inhibition, *J. Colloid Interface Sci*, **516**: 511–521 (2018).

[16] Abdul M., Devadi H., Krishna M., Narasimh H.N., Sathyanarayana M.B.S., Statistical Optimization for Photocatalytic Degradation of Methylene Blue by Ag-TiO$_2$ Nanoparticles, *Procedia Materials Science*, 5(2014) 612-621.

[17] Vaiano V., Sacco O., Sannino D., Electric Energy Saving In Photocatalytic Removal of Crystal Violet Dye Through the Simultaneous use of Long-Persistent Blue Phosphors, Nitrogen-Doped TiO$_2$ and UV-Light Emitting Diodes, *J. Clean. Prod*, **210**: 1015–1021 (2019).

[18] Mosleh S., Rahimi M.R., Ghaedi M., Dashtian K., Hajati S., Wang S., Ag$_3$PO$_4$/AgBr/Ag-HKUST-1-MOF composites as Novel Blue LED Light Active Photocatalyst for Enhanced Degradation of Ternary Mixture of Dyes in a Rotating Packed Bed Reactor, *Chem. Eng. Process*, **114**: 24-38 (2017).

[19] Wang X., Lim T., Solvothermal Synthesis of C–N Codoped TiO$_2$ and Photocatalytic Evaluation for Bisphenol A Degradation Using a Visible-Light Irradiated LED Photoreactor, *Appl. Catal. B*, **100**: 355–364 (2010).

[20] Hossaini H., Moussavi G., Farrokhi M., The Investigation of the LED-Activated FeFNS-TiO$_2$ Nanocatalyst for Photocatalytic Degradation and Mineralization of Organophosphate Pesticides in Water, *Water Res*, **59**: 130–144 (2014).

[21] Subagio D.P., Srinivasan M., Lim M., Lim T.T., Photocatalytic Degradation of Bisphenol-A by Nitrogen-Doped TiO$_2$ Hollow Sphere in a vis-LED Photoreactor, *Appl. Catal. B.*, **95**: 414–422 (2010).

[22] Lei P., Wang F., Gao X., Ding Y., Zhang S., Zhao J., Liu S., Yang M., Immobilization of TiO$_2$ Nanoparticles in Polymeric Substrates by Chemical Bonding for Multi-Cycle Photodegradation of Organic Pollutants, *J. Hazard. Mater*, **227–228**: 185–194 (2012).

[23] He T., Ma H., Zhou Z., Xu W., Ren F., Shi Z., Wang J., Preparation of ZnS Fluor Polymer Nano Composites and its Photocatalytic Degradation of Methylene Blue, *Polym. Degrad. Stab.*, **94**: 2251–2256 (2009).

[24] Chahkandi M., Zargazi M., New Water Bbased EPD Thin BiVO$_4$ Film: Effective Photocatalytic Degradation of Amoxicillin Antibiotic, *J. Hazard. Mater*, **12**: 18-50 (2019).

[25] Chen W., Chu M., Gao L., Mao L., Yuan J., Shangguan W., Ni(OH)$_2$ Loaded on TaON for Enhancing Photocatalytic Water Splitting Activity Under Visible Light Irradiation, *Appl. Surf. Sci.*, **324**: 432-437 (2015b).

[26] Vereb G., Ambrus Z., Pap Z., Mogyorosi K., Dombi A., Hernadi K., Immobilization of Crystallized Photocatalysts on Ceramic Paper by Titanium (IV) Ethoxide and Photocatalytic Decomposition of Phenol, *React. Kinet, Mech, Catal*, **113**: 293-303 (2014).

[27] Jansson I., Yoshiiri K., Hori H., García-García F.J., Rojas S., Sanchez B., Ohtani B., Suarez S., Visible Light Responsive Zeolite/WO$_3$/Pt Hybrid Photocatalysts for Degradation of Pollutants in Air, *Appl. Catal. A*, **521**: 208-219 (2016).

[28] Shan A.Y., Immobilisation of Titanium Dioxide onto Supporting Materials in Heterogeneous Photocatalysis: A Review, *Appl. Catal. A, General*, **2**: 1-8 (2010).

[29] Xuzhuang Y., Yang D., Huaiyong Z., Jiangwen L., Martins W.N., Frost R., Daniel L., Yuenian S., Mesoporous Structure with Size Controllable Anatase Attached on Silicate Layers for Efficient Photocatalysis, *J. Phys. Chem. C*, **113**: 8243-8248 (2009).

[30] Barati N., Faghihi Sani M.A., Ghasemi H., Sadeghian Z., Mirhoseini S.M.M., Preparation of Uniform TiO$_2$ Nanostructure Film on 316L Stainless Steel by Sol–Gel Dip Coating, *Appl. Surf. Sci*, **255**: 8328–8333 (2009).

[31] Matsumura T., Noshiroy D., Tokumur M., Znad H.T., Kawase Y., Simplified Model for the Hydrodynamics and Reaction Kinetics in a Gas−Liquid−Solid Three-Phase Fluidized-Bed Photocatalytic Reactor: Degradation of -Cresol with Immobilized TiO$_2$, *Ind. Eng. Chem. Res*, **46**: 2637-2647 (2007).

[32] Boiarkina I., Norris S., Patterson D.A., Investigation into the Effect of Flow Structure on the Photocatalytic Degradation of Methylene Blue and Dehydroabietic Acid in a Spinning Disc Reactor, *Chem. Eng. J.,* **222**: 159-171 (2013).

[33] Caprariis B., Rita M. Di, Stoller M., Verdone N., Chianese A., Reaction-Precipitation by a Spinning Disc Reactor: Influence of Hydrodynamics on Nanoparticles Production, *Chem. Eng. J.,* **76**: 73-80 (2012).

[34] Stephan B., Ludovic L., Dominique W., Modelling of a Falling Thin Film Deposited Photocatalytic Step Reactor for Water Purification: Pesticide Treatment, *Chem. Eng. J.,* **169**: 216–225 (2011).

[35] Chong M.N., Jin B., Chow C.W.K., Sol–GelSaint C., Recent Developments in Photocatalytic Water Treatment Technology: A Review, *Water. Res*, **44**: 2997–3027 (2010).

[36] Bagheri S., Ghaedi M., Asfaram A., Alipanahpour Dil E., Javadian H., RSM-CCD Design of Malachite Green Adsorption onto Activated Carbon with Multimodal Pore Size Distribution Prepared from Amygdalus Scoparia: Kinetic and Isotherm Studies, *Polyhedron*, **171**: 464-472 (2019).

[37] Lu Y., Zhang X., Chu Y., Yu H., Huo M., Qu J., Crittenden J.C., Huo H., X. Yuan, Cu_2O Nanocrystals/TiO_2 Microspheres Film on a Rotating Disk Containing Long-Afterglow Phosphor for Enhanced Round-the-Clock Photocatalysis, *Appl. Catal. B*, **224**: 239-248 (2018).

[38] Vilardi G., Stoller M., Verdone N., Di Palma L., Production of Nano Zero Valent Iron Particles by Means of a Spinning Disk Reactor, *Chem. Eng. Trans*, **57**: 1865-1859 (2017).

[39] Bahmani M., Dashtian K., Mowla D., Esmaeilzadeh F., Ghaedi M., UiO-66(Ti)-Fe_3O_4-WO_3 Photocatalyst for Efficient Ammonia Degradation from Wastewater into Continuous Flow-Loop Thin Film Slurry Flat-Plate Photoreactor, *J. Hazard. Mater*, **393**: 1-13 (2020).

[40] Mosleh S., Rahimi M.R., Ghaedi M., Dashtian K., Hajati S., Photocatalytic Degradation of Binary Mixture Of Toxic Dyes by HKUST-1 MOF and HKUST-1-SBA-15 in a Rotating Packed Bed Reactor under Blue LED Illumination: Central Composite Design Optimization, *R. S. C. Advances*, **6**: 17204–17214 (2016a).

Research Article